Title	Time integration in linear viscoelasticity - a comparative study
Author(s)	Sorvari, Joonas; Hämäläinen, Jari
Citation	Mechanics of Time-Dependent Materials - article in press
Date	2010
URL	http://dx.doi.org/10.1007/s11043-010-9108-7
Rights	Copyright © Springer. This article may be downloaded for personal use only

Noname manuscript No.
(will be inserted by the editor)

Time integration in linear viscoelasticity - a comparative study

Joonas Sorvari · Jari Hämäläinen

Received: date / Accepted: date

Abstract One of the key tasks in computational viscoelasticity is the time integration of the constitutive equation. It is important that the behaviour of the integrators is well understood since they are used in a variety of applications. In the present paper, the performance of conventional semi-analytical methods and implicit Runge-Kutta methods for the integral model of linear viscoelasticity with Prony series is evaluated analytically and numerically. Although a linear viscoelastic constitutive equation is considered, the analyzed integrators can be extended to handle also Schapery-type nonlinear constitutive equations. Numerical examples involving a simple uniaxial problem and multiaxial simulations are presented in order to analyze and compare the time integrators.

Keywords linear viscoelasticity · time integration · semi-analytical methods · implicit Runge-Kutta methods · Maxwell model

1 Introduction

Efficient time integrators may be needed in deterministic parameter estimation methods (Goh et al., 2004; Sorvari and Malinen, 2007), in interconversion methods (Dooling et al., 1997; Touati and Cederbaum, 1998) as well as in finite element method (Poon and Ahmad, 1998, 1999). Thus, one of the key issues in computational viscoelasticity is the time integration of viscoelastic constitutive equations.

The response of a viscoelastic material depends on the excitation history. For the integral models of viscoelasticity, the entire excitation history must be kept in memory in order to evaluate the response numerically. Therefore, the memory storage increases in time. The storage problem can be avoided by representing the kernel function as a Prony series. Due to the semigroup property of the exponential function, i.e. $\exp(a+$

J. Sorvari
VTT Technical Research Centre of Finland, P.O. Box 1000, 02044 VTT, Finland
E-mail: joonas.sorvari@vtt.fi

J. Hämäläinen
Department of Physics, University of Kuopio, P.O. Box 1627, 70211 Kuopio, Finland
E-mail: jari.hamalainen@uku.fi

$b) = \exp(a)\exp(b)$ for any constants a and b, the use of a Prony series enables an efficient recursive relation to be derived (Simo and Hughes, 1998). In conventional time integration methods, the Prony series representation is combined with a simplified assumption of the loading program within a time increment. For example, constant (Zienkiewicz et al., 1968), piecewise constant (Herrman and Peterson, 1968), linear (Taylor et al., 1970) and even exponential (Argyris et al., 1991) time variation of the excitation history have been used. Similar integration methodologies have also been succesfully applied for Schapery's nonlinear viscoelastic model (Henriksen, 1984; Beijer and Spoormaker, 2002), for the Duvaut-Lions viscoplasticity model (Simo et al., 1988), in large strain viscoelasticity (Holzapfel, 1996) and in endochronic plasticity (Hsu et al., 1991) as well as in other application areas (Patlashenko et al., 2001).

When the kernel function is represented via the Prony series, the problem of integrating the viscoelastic constitutive equation can be converted to the problem of integrating an evolution equation of a Maxwell element, which is a first order differential equation. From the differential perspective the conventional linear viscoelastic time integration strategies can be interpreted as exponential time differencing (ETD) schemes (Beylkin et al., 2002; Cox and Matthews, 2002), which have recently been extensively studied in the area of computational physics. The idea in the exponential time differencing is to integrate the linear part of the first order differential equation exactly and to approximate the (nonlinear) source term by an algebraic polynomial. According to Poon and Ahmad (1998), the differential approach enables flexibility in choosing of a suitable time integration method and obviates the need for a non-physical simplified loading program within a time step. However, this approach has not gained popularity, few exceptions being Poon and Ahmad (1998, 1999); Gramoll et al. (1989). In literature (Zienkiewicz and Taylor, 2000; Beijer and Spoormaker, 2002) the conventional semi-analytical methods are considered superior over the typical low-order Runge-Kutta methods. For (visco)plastic constitutive models, a variety of integrators have been successfully applied, such as the backward Euler method (Schreyer et al., 1979), implicit Runge-Kutta methods (Büttner, 2002), Rosenbrock methods (Kirchner and Kollmann, 1999), BDF methods (Kirchner and Simeon, 1999), etc. From this perspective, one might wonder why the common solution methods of ordinary differential equations have not gained popularity. If the generalized trapezoidal rule is considered, the reasons seem to be rather clear. The stable backward Euler method is asymptotically only first-order accurate and the second-order accurate trapezoidal method yields spurious numerical oscillations when the time step is large. However, the answer is not so straightforward as it may seem. When the time step is large, the backward Euler method may perform better than higher-order methods (Kouhia et al., 2005), and further, the oscillation of the trapezoidal method can be reduced in several ways (Østerby, 2003).

Although the time integration in linear viscoelasticity can be considered to be rather well established, it seems that rather little is known about discrepancies and advantages of the different integrators. In addition, integrators of the linear model are often extended to handle also nonlinear viscoelastic models. For nonlinear models the choice of the method is far from obvious. In fact, the motivation for this research stems from the problem of integrating Schapery's (Schapery, 1969, 1997) nonlinear viscoelastic model.

The aim of the present paper is to add understanding to the behavior of the different time integrators so that even a nonspecialist rheologist programmer would be capable of choosing a proper integrator from among the large arsenal of methods. Be-

sides evaluating the performance of conventional methods, the performance of implicit Runge-Kutta methods is evaluated. The analysis ranges from a local error analysis of a uniaxial model to a multiaxial FEM simulation.

2 Time integrators

The evolution equation of a Maxwell element is given by

$$\frac{d\sigma^*(t)}{dt} = -\frac{1}{\lambda}\sigma^*(t) + E\frac{d\varepsilon(t)}{dt}, \quad \sigma^*(0) = E\varepsilon(0), \tag{1}$$

where σ^* is the internal stress, $\lambda > 0$ is the relaxation time and $E > 0$ is the stiffness modulus of the element. A Maxwell system consists of several Maxwell elements connected in parallel. The total stress of the system is given by the sum of the internal stresses. For engineering materials the relaxation process evolves on several time scales and thus the range of relaxation times may be very wide in a Maxwell system. The relaxation times are commonly chosen *a priori*, for example, equidistantly on the logarithmic time axis one or two per decade of experimental data (Knauss and Zhao, 2007). The value for the ratio between the largest and the smallest relaxation time, i.e. $\lambda_{\max}/\lambda_{\min}$, can be 10^{10} or even higher for a Maxwell system. Therefore, a suitable integrator should be stable and accurate for both small and large values of λ.

Due to stability restrictions the use of conventional explicit integrators, such as the forward Euler method, leads to impractically small time steps to be used in practical analysis. Roughly speaking, a typical explicit integrator has a critical time step of order $\lambda_{\min}$ for a Maxwell system. Clearly, the use of implicit integrators is a necessity.

In a stiff case, characterized by $\lambda << 1$, the solution of the evolution equation consists of two phases: a fast phase where there is a rapid approach to a slow manifold followed by a slow phase where the solution evolves along the slow manifold (Cox and Matthews, 2002), see Fig. 1. In the slow manifold the internal stress is given by (Cox and Matthews, 2002; Boyd, 2001)

$$\sigma^*(t) = E\lambda\frac{d\varepsilon}{dt} - E\lambda^2\frac{d^2\varepsilon}{dt^2} + E\lambda^3\frac{d^3\varepsilon}{dt^3} - + \dots \tag{2}$$

for the Maxwell model.

Since the ordinary differential equation (ODE) (1) involves a time derivative of the strain, it is advantageous for numerical purposes to transform the ODE to form

$$y'(t) = F(t, y(t)) = -\frac{1}{\lambda}y(t) + \frac{E}{\lambda}\varepsilon(t) \tag{3}$$

by using a change of variables $\sigma^*(t) = E\varepsilon(t) - y(t)$. The numerical scheme of the transformed ODE can be transformed back to the original variable σ^* by using again the change of variables. The naming convention of the integrators is based on the integrators of the transformed ODE (3).

2.1 Runge-Kutta methods

An s-stage implicit Runge-Kutta (RK) method for the transformed ODE (3) is given by

$$y_{n+1} = y_n + \Delta t \sum_{i=1}^{s} b_i k_i, \tag{4}$$

$$k_i = F\left(t_n + c_i \Delta t, y_n + \Delta t \sum_{j=1}^{s} a_{ij} k_j\right) \quad i = 1, \ldots, s, \tag{5}$$

where a_{ij}, b_i, c_i are the coefficients of the method and $\Delta t = t_{n+1} - t_n$ is the step-size. The backward Euler method for the Maxwell model is given by

$$\sigma^*_{n+1} = \frac{1}{1 + \Delta t/\lambda}\sigma^*_n + \frac{E\Delta\varepsilon}{1 + \Delta t/\lambda} \qquad \text{(bE)}, \tag{6}$$

where $\Delta\varepsilon = \varepsilon(t_{n+1}) - \varepsilon(t_n)$ is the strain increment[1]. The trapezoidal or two-stage Lobatto IIIA method is given by

$$\sigma^*_{n+1} = \frac{1 - \frac{1}{2}\Delta t/\lambda}{1 + \frac{1}{2}\Delta t/\lambda}\sigma^*_n + \frac{E\Delta\varepsilon}{1 + \frac{1}{2}\Delta t/\lambda} \qquad \text{(Tr)}, \tag{7}$$

and the two-stage Lobatto IIIC method by

$$\sigma^*_{n+1} = \frac{\sigma^*_n + (1 + \frac{1}{2}\Delta t/\lambda)E\Delta\varepsilon}{1 + \Delta t/\lambda + \frac{1}{2}(\Delta t/\lambda)^2} \qquad \text{(L3C)}. \tag{8}$$

According to Kouhia et al. (2005), the integrator of an inelastic material model should be at least L-stable, and for the ODE (1) without the source term, the amplification factor should be positive and monotonous. Both the backward Euler and Lobatto IIIC methods fulfil these criteria. However, the trapezoidal method is only A-stable, i.e. the amplification factor of the trapezoidal method doesnt't approach zero as $\Delta t/\lambda \to \infty$. Nevertheless, as it is well known, the trapezoidal method is a good choice if the time step is sufficiently small. For more details on Lobatto methods and stability properties of RK methods we refer to Hair and Wanner (1991).

The considered RK methods are closely related to Galerkin methods in time. The backward Euler and trapezoidal methods can also be derived by applying the Galerkin methods directly to the ODE (1). The backward Euler is equivalent to the discontinuous Galerkin method of degree zero and the trapezoidal method is equivalent to the continuous Petrov-Galerkin method of degree one[2]. The performance of several Galerkin methods for creep type inelastic models has been evaluated in Reference Kouhia et al. (2005).

We would like to emphasize that the RK methods can be extended to handle thermal (thermorheologically simple models) and nonlinear (Schapery type models) effects as long as the kernel function is represented via the Prony series, i.e. constitutive equation can be expressed in differential form.

[1] $(\bullet)(t_m)$ denotes the exact solution at time t_m whereas $(\bullet)_m$ denotes the numerical solution at time t_m, $m \in \{n, n+1\}$.

[2] For the Galerkin methods we use definitions given in Reference Kouhia et al. (2005).

2.2 Semi-analytical methods

For viscoelastic materials the most popular time integrators are based on idealized loading programs in which simplified variation of strain is assumed within a time step. In what follows we adopt the name semi-analytical (SA) integrators for these types of methods. To be more specific, we define SA integrators as methods in which the evolution equation is integrated exactly by approximating strain by a continuous or discontinuous polynomial within a time step.

The exact solution for the transformed ODE is given by

$$y(t_{n+1}) = e^{-\Delta t/\lambda} y(t_n) + \frac{E}{\lambda} \int_{t_n}^{t_{n+1}} e^{-(t_{n+1}-\tau)/\lambda} \varepsilon(\tau) d\tau. \tag{9}$$

The simplest approximation to evaluate the integral analytically is to assume that the strain is constant throughout the time interval. Approximating $\varepsilon(\tau)$ in a backward manner, i.e. $\varepsilon(\tau) = \varepsilon_{n+1}$, and transforming the resulting scheme to the original variable yields

$$\sigma^*_{n+1} = e^{-\Delta t/\lambda} \sigma^*_n + e^{-\Delta t/\lambda} E \Delta\varepsilon \qquad \text{(SA1)}. \tag{10}$$

The SA1 method was first introduced by Zienkiewicz et al. (1968) for a Kelvin system.

A better approximation to the integral is to assume piecewise constant variation of strain which gives

$$\sigma^*_{n+1} = e^{-\Delta t/\lambda} \sigma^*_n + e^{-\Delta t/(2\lambda)} E \Delta\varepsilon \qquad \text{(SA2)}. \tag{11}$$

This scheme is often derived by integrating the evolution equation exactly (see Eq. (18)) and then using the midpoint rule to the integral and the center difference scheme to the time derivative of strain, see e.g. Simo and Hughes (1998) and also Feng (1992).

Rather than approximating strain in a constant manner, we may approximate the strain rate to be constant. Linear variation of strain gives

$$\sigma^*_{n+1} = e^{-\Delta t/\lambda} \sigma^*_n + \frac{1 - e^{-\Delta t/\lambda}}{\Delta t/\lambda} E \Delta\varepsilon \qquad \text{(SA3)}. \tag{12}$$

The SA3 method is commonly attributed to Taylor et al. (1970). For small $\Delta t/\lambda$ the second term of the right-hand side of Eq. (12) suffers from cancellation error. Thus, to avoid rounding errors a series expansion should be used when $\Delta t/\lambda$ is small

$$\frac{1 - e^{-\Delta t/\lambda}}{\Delta t/\lambda} = 1 - \frac{1}{2}\left(\frac{\Delta t}{\lambda}\right) + \frac{1}{6}\left(\frac{\Delta t}{\lambda}\right)^2 - + \ldots. \tag{13}$$

The considered SA schemes have also been extended to nonlinear viscoelastic models. The constant and piecewise constant schemes have been generalized to the nonlinear creep-based Schapery's model by Beijer and Spoormaker (2002). For Schapery's model a time integration method which reduces in a linear case to the SA3 method was derived by Henriksen (1984) and has been used by many other researchers (Czyz and Szyszkowski, 1999; Lai and Bakker, 1996; Kennedy, 1998; Haj-Ali and Muliana, 2004).

Rather interestingly, we see that the only difference between the SA3 method and the trapezoidal and Lobatto IIIC methods is the order of approximation of the exponential function. We may rewrite Eqs. (7), (8) and (12) as

$$\sigma^*_{n+1} = Q(-\Delta t/\lambda) \sigma^*_n + \frac{1 - Q(-\Delta t/\lambda)}{\Delta t/\lambda} E \Delta\varepsilon, \tag{14}$$

where $Q(z)$ is the exponential function for the SA3 method, the diagonal (1,1)-Padé approximation for the trapezoidal method and the subdiagonal (0,2)-Padé approximation for the Lobatto IIIC method. Similarly, we see that the SA1 method reduces to the backward Euler method when the (0,1)-Padé approximation is used to the exponential.

Another interesting observation can be made when λ is small. In that case the first term in the series (2) is recovered for the SA3 method as well as for the backward Euler and Lobatto IIIC methods. Note the interesting behavior of the backward Euler method. For large λ the backward Euler method approaches the SA1 method while for small λ the backward Euler method approaches the SA3 method.

2.3 Integrating factor methods

Yet another possible approach is the direct numerical integration of the integral in Eq. (9). At first glance, this might seem to be a promising alternative. However, as we will soon see, a direct numerical integration is not generally a good choice. This kind of approach has been used for example in Oden and Armstrong (1971) where the Simpson's rule was used for a thermoviscoelastic model, see also Rivkin and Givoli (2000). These methods can be identified as integrating factor (IF) methods (Minchev and Wright, 2005) where the ODE (3) is transformed to form

$$\frac{d}{dt}\left(ye^{t/\lambda}\right) = \frac{E}{\lambda}\varepsilon(t)e^{t/\lambda}, \tag{15}$$

and then a RK method is applied to the ODE. Applying the generalized trapezoidal rule to (15) and transforming the resulting scheme to the original variable σ^* yields the generalized IF trapezoidal rule

$$\begin{aligned}\sigma^*_{n+1} = e^{-\Delta t/\lambda}\sigma^*_n &+ E\varepsilon(t_{n+1})(1-\theta\Delta t/\lambda)\\ &-E\varepsilon(t_n)(1+[1-\theta]\Delta t/\lambda)e^{-\Delta t/\lambda}.\end{aligned} \tag{16}$$

The cases $\theta = 0$, $\theta = 1/2$ and $\theta = 1$ corresponds to forward, trapezoidal, and backward integration of the integral in Eq. (9)

To demonstrate a weakness in the IF methods we consider a problem with constant strain. It is most important that a time integrator of the viscoelastic model behaves correctly in this simple stress relaxation problem. When the strain is constant, the local error for the generalized IF trapezoidal rule is given by

$$\begin{aligned}\mathcal{E} &\equiv \sigma^*(t_{n+1}) - \sigma^*_{n+1}\\ &= -E\varepsilon\left((1-\theta\Delta t/\lambda) - (1+[1-\theta]\Delta t/\lambda)e^{-\Delta t/\lambda}\right).\end{aligned} \tag{17}$$

For $\Delta t/\lambda >> 1$ the error is $\sim \theta\Delta t/\lambda$ indicating a linear growth of the error except for the forward IF Euler which is accurate at limit $\Delta t/\lambda \to \infty$. It can also be shown that if Simpson's rule is applied to Eq. (9), $\mathcal{E} \to \infty$ at the limit. Clearly, we cannot use integration rules which have integration point at the right end point of the interval, i.e. at t_{n+1}. Therefore, the only practical choice is the forward IF Euler method which, however, is far more less accurate than the SA methods. Consequently, in the forthcoming sections, the analysis is concentrated only on the SA and RK methods. Finally, we point out that the poor performance of the IF methods has been reported in other application areas as well, see e.g. Cox and Matthews (2002).

3 Local error analysis

For the local error analysis we follow the approach taken in Reference Kværnø (2004). In addition, it is assumed that the strain is independent of relaxation time λ.

The exact solution for the evolution equation of a Maxwell element is given by

$$\sigma^*(t_{n+1}) = e^{-\Delta t/\lambda}\sigma^*(t_n) + Ee^{-\Delta t/\lambda}\int_0^{\Delta t} e^{\tau/\lambda}\frac{d}{d\tau}\varepsilon(t_n+\tau)d\tau. \tag{18}$$

Without loss of generality, we may assume hereafter that $E = 1$ or equivalently we may consider the dimensionless form of the evolution equation. By expanding $\varepsilon(t_n+\tau)$ into a Taylor series gives

$$\begin{aligned}\sigma^*(t_{n+1}) = e^{-\Delta t/\lambda}\sigma^*(t_n) + \sum_{k=1}^{\infty}\varepsilon^{(k)}(t_n)\frac{1}{(k-1)!}\\ \times\, e^{-\Delta t/\lambda}\int_0^{\Delta t} e^{\tau/\lambda}\tau^{k-1}d\tau.\end{aligned} \tag{19}$$

After integrating each term separately, we get

$$\sigma^*(t_{n+1}) = \varphi_0(\Delta t/\lambda)\sigma^*(t_n) + \sum_{k=1}^{\infty}\varphi_k(\Delta t/\lambda)\varepsilon^{(k)}(t_n)\Delta t^k, \tag{20}$$

where

$$\varphi_k(z) = \frac{1}{(-z)^k}\left(e^{-z} - \sum_{j=0}^{k-1}\frac{(-z)^j}{j!}\right) \qquad k = 1, 2, \ldots, \tag{21}$$

and $\varphi_0(z) = \exp(-z)$ by definition.

The RK and SA methods can be written in a uniform form as

$$\sigma^*_{n+1} = \psi_0(\Delta t/\lambda)\sigma^*_n + \psi_1(\Delta t/\lambda)E\Delta\varepsilon. \tag{22}$$

In the following, it is assumed that the exact solution is known at time t_n, i.e. $\sigma^*_n = \sigma^*(t_n)$. Functions $\psi_0(z)$ and $\psi_1(z)$ for the methods are given in Table 1. By expanding $\varepsilon(t_{n+1})$ we arrive at the following formula

$$\sigma^*_{n+1} = \psi_0(\Delta t/\lambda)\sigma^*(t_n) + \sum_{k=1}^{\infty}\psi_k(\Delta t/\lambda)\varepsilon^{(k)}(t_n)\Delta t^k, \tag{23}$$

where $\psi_k(z) = \dfrac{\psi_1(z)}{k!}$.

By subtracting Eq. (23) from Eq. (20) we obtain the local truncation error

$$\begin{aligned}\sigma^*(t_{n+1}) - \sigma^*_{n+1} = \mathcal{E}_0(\Delta t/\lambda)\sigma^*(t_n)\\ + \sum_{k=1}^{\infty}\mathcal{E}_k(\Delta t/\lambda)\varepsilon^{(k)}(t_n)\Delta t^k,\end{aligned} \tag{24}$$

where the error function is $\mathcal{E}_k(z) = \varphi_k(z) - \psi_k(z)$. When $\sigma^*(t_n)$ is on the slow manifold (see Eq. (2)), then the truncation error is

$$\sigma^*(t_{n+1}) - \sigma^*_{n+1} = \sum_{k=1}^{\infty}\widetilde{\mathcal{E}}_k(\Delta t/\lambda)\varepsilon^{(k)}(t_n)\Delta t^k, \tag{25}$$

where $\widetilde{\mathcal{E}}_k(z) = \mathcal{E}_k(z) - \mathcal{E}_0(z)/(-z)^k$.

3.1 Nonstiff case

In the nonstiff case, $\Delta t/\lambda << 1$, we express the error functions in terms of a Taylor series expansion. The dominant terms of the error functions are given in Tables 2 and 3. Then, by inserting the dominant terms into the truncation error equation we obtain the local errors. For the first-order accurate methods the errors are given by

$$\mathcal{E}_{\mathrm{bE}} \approx \frac{1}{2} \cdot \frac{1}{\lambda^2} \left[-\sigma^*(t_n) + \lambda \varepsilon'(t_n) \right] \Delta t^2, \tag{26}$$

$$\mathcal{E}_{\mathrm{SA1}} \approx \frac{1}{2} \cdot \frac{1}{\lambda} \varepsilon'(t_n) \Delta t^2, \tag{27}$$

and for the higher-order methods

$$\mathcal{E}_{\mathrm{Tr}} \approx \frac{1}{12} \cdot \frac{1}{\lambda^3} \left[\sigma^*(t_n) - \lambda \varepsilon'(t_n) + \lambda^2 \varepsilon''(t_n) \right] \Delta t^3, \tag{28}$$

$$\mathcal{E}_{\mathrm{L3C}} \approx \frac{1}{12} \cdot \frac{1}{\lambda^3} \left[-2\sigma^*(t_n) + 2\lambda \varepsilon'(t_n) + \lambda^2 \varepsilon''(t_n) \right] \Delta t^3, \tag{29}$$

$$\mathcal{E}_{\mathrm{SA2}} \approx \frac{1}{12} \cdot \frac{1}{\lambda^2} \left[\frac{1}{2} \varepsilon'(t_n) + \lambda \varepsilon''(t_n) \right] \Delta t^3, \tag{30}$$

$$\mathcal{E}_{\mathrm{SA3}} \approx \frac{1}{12} \cdot \frac{1}{\lambda} \varepsilon''(t_n) \Delta t^3. \tag{31}$$

The results are as expected. When $\lambda << 1$ and $\sigma^*(t_n)$ is on the slow manifold, the errors for the RK methods are given by

$$\mathcal{E}_{\mathrm{bE}} \approx \left[\frac{1}{2} \varepsilon''(t_n) + \mathcal{O}(\lambda) \right] \Delta t^2, \tag{32}$$

$$\mathcal{E}_{\mathrm{Tr}} \approx \left[\frac{1}{12} \varepsilon'''(t_n) + \mathcal{O}(\lambda) \right] \Delta t^3, \tag{33}$$

$$\mathcal{E}_{\mathrm{L3C}} \approx \left[\frac{1}{4} \frac{1}{\lambda} \varepsilon''(t_n) - \frac{1}{6} \varepsilon'''(t_n) + \mathcal{O}(\lambda) \right] \Delta t^3. \tag{34}$$

In this case the error of the backward Euler and trapezoidal methods is almost independent of λ whereas for the Lobatto IIIC method the error behaves similarly as for the SA3 method.

3.2 Stiff case

In the stiff case, $\Delta t/\lambda >> 1$, we ignore the exponential terms and expand the error functions as a function of $(\Delta t/\lambda)^{-1}$. The dominant terms are given in Tables 4 and 5. The local errors are now given by

$$\mathcal{E}_{\mathrm{L3C}} \approx 2\lambda^2 \left[-\sigma^*(t_n) + \lambda \varepsilon'(t_n) \right] \frac{1}{\Delta t^2}, \tag{35}$$

$$\mathcal{E}_{\mathrm{bE}} \approx \lambda \left[-\sigma^*(t_n) + \lambda \varepsilon'(t_n) \right] \frac{1}{\Delta t}, \tag{36}$$

$$\mathcal{E}_{\mathrm{Tr}} \approx \sigma^*(t_n) - \lambda \varepsilon'(t_n) + \lambda^2 \varepsilon''(t_n), \tag{37}$$

$$\mathcal{E}_{\mathrm{SA1}} \approx \lambda \varepsilon'(t_n), \tag{38}$$

$$\mathcal{E}_{\mathrm{SA2}} \approx \lambda \varepsilon'(t_n), \tag{39}$$

$$\mathcal{E}_{\mathrm{SA3}} \approx \frac{1}{2} \lambda \varepsilon''(t_n) \Delta t. \tag{40}$$

The local errors behave rather differently as a function of the time step. For the backward Euler and for Lobatto IIIC methods, the error decreases as the step size increases. For the trapezoidal, SA1 and SA2 methods the leading error term is independent of the time step. In addition, the error is approximately the same for the SA1 and SA2 methods. Once again, the best choice seems to be the SA3 method. However, in the slow manifold case the error of the trapezoidal method has a quadratic dependency on the time step

$$\mathcal{E}_{\mathrm{bE}} \approx \mathcal{E}_{\mathrm{L3C}} \approx \frac{1}{2}\lambda\varepsilon''(t_n)\Delta t, \tag{41}$$

$$\mathcal{E}_{\mathrm{Tr}} \approx \frac{1}{6}\lambda\varepsilon'''(t_n)\Delta t^2, \tag{42}$$

Furthermore, the error is now the same for the SA3, backward Euler and Lobatto IIIC methods.

3.3 A numerical example

We consider a differential equation

$$\frac{d\sigma^*(t)}{dt} = -\frac{1}{\lambda}\sigma^*(t) + \frac{d}{dt}(-\cos t), \qquad \sigma^*(t_0) = \sigma_0^*, \tag{43}$$

with initial conditions

$$\sigma_0^* = 1 \qquad \text{(off the slow manifold)}, \tag{44}$$

$$\sigma_0^* = \frac{\lambda}{1+\lambda^2}(\sin t_0 - \lambda\cos t_0) \qquad \text{(on the slow manifold)}. \tag{45}$$

where $t_0 = \pi/4$. The exact solution is given by

$$\sigma^*(t) = \left(\sigma_0^* - \frac{\lambda}{1+\lambda^2}(\sin t_0 - \lambda\cos t_0)\right) e^{-(t-t_0)/\lambda} + \frac{\lambda}{1+\lambda^2}(\sin t - \lambda\cos t). \tag{46}$$

The errors after one time step are shown in Fig. 2. The numerical results are in accordance with the theoretical predictions. We see that in the stiff case the error is almost the same for the SA1 and SA2 methods and for the backward Euler and Lobatto IIIC methods the error decreases as the time step increases. In the slow manifold case we see that the error is approximately the same for the backward Euler, Lobatto IIIC and SA3 methods when $\Delta t/\lambda >> 1$. In addition, the trapezoidal method produces the lowest error.

4 Uniaxial Maxwell solid

4.1 Constitutive model

We consider a linearly viscoelastic constitutive equation of the form

$$\sigma(t) = \int_{-\infty}^{t} E(t-\tau)\dot{\varepsilon}(\tau)d\tau, \tag{47}$$

with a kernel function

$$E(t) = E_\infty + (E_0 - E_\infty)e^{-t/\lambda}, \tag{48}$$

where E_∞ is the long-term modulus and E_0 is the instantaneous modulus. The model represents the standard linear viscoelastic solid in which a Maxwell element is connected in parallel to a Hookean spring. Alternatively, the constitutive equation can be written as

$$\sigma(t) = E_\infty \varepsilon(t) + \sigma^*(t), \tag{49}$$

where the evolution of the internal stress is given by Eq. (1) with $E = E_0 - E_\infty$. The numerical solution for the internal stress is given by Eq. (22).

In the following we analyze the performance of the integrators in typical experiments which are most likely encountered in practice. We consider two strain-based experiments

$$\varepsilon(t) = \varepsilon_0, \tag{50}$$

$$\varepsilon(t) = \dot{\varepsilon}_0 t, \tag{51}$$

and a stress-based experiment (creep, $\sigma(t) = \sigma_0$)

$$\varepsilon(t) = \frac{\sigma_0}{(E_0 - E_\infty)} \left(1 - (1-\eta)e^{-\eta t/\lambda}\right)(1/\eta - 1), \tag{52}$$

where $\eta = E_\infty/E_0 \in (0,1)$ is a dimensionless parameter. For elastic materials we would have $\eta = 1$ whereas for viscoelastic liquid $\eta = 0$. Although we consider also a stress-based experiment, we study a strain-driven problem in which the stress is regarded as the unknown variable. Further, we are mainly interested in cases in which $\Delta t/\lambda$ is relatively large, say greater than one. For values $\Delta t/\lambda << 1$ we may expect the integrators to behave according to the local error analysis given in Section 3.1.

4.2 Relaxation

For this problem the SA methods yield exact results. For the RK methods we characterized the performance of the integrators in terms of an amplification factor, i.e. ratio $\sigma^*_{n+1}/\sigma^*_n$, which are

$$A_{\mathrm{bE}} = \frac{1}{1 + \Delta t/\lambda}, \tag{53}$$

$$A_{\mathrm{Tr}} = \frac{1 - \frac{1}{2}\Delta t/\lambda}{1 + \frac{1}{2}\Delta t/\lambda}, \tag{54}$$

$$A_{\mathrm{L3C}} = \frac{1}{1 + \Delta t/\lambda + \frac{1}{2}(\Delta t/\lambda)^2}. \tag{55}$$

The exact amplification factor is $\exp(-\Delta t/\lambda)$. The amplification factors are shown in Fig. 3. The backward Euler and Lobatto IIIC methods are accurate for both very small and large time steps. Trivially, at limit $\Delta t/\lambda \to \infty$ the A-stable trapezoidal method is inaccurate. However, in the nonstiff case the trapezoidal method is more accurate than

- the backward Euler when $\Delta t/\lambda \lesssim 2.6$,
- the Lobatto IIIC when $\Delta t/\lambda \lesssim 0.9$,

when measured by $|A_{\mathrm{exact}} - A_{\mathrm{num}}|$. We note that when $\Delta t/\lambda > 2$, the amplification factor of the trapezoidal method is negative and in that case the trapezoidal method produces oscillations.

4.3 Constant strain rate problem

To begin with, we illustrate in Fig. 4 the typical performance of the integrators in a constant strain rate case. The numerical solution of the backward Euler and Lobatto IIIC methods follows the true solution smoothly whereas for the SA1 and SA2 methods the numerical solution diverges from the true solution after the transient phase. The most notable difference is observed between the backward Euler and SA2 methods. After the transient phase, asymptotically only first-order accurate Euler scheme is more accurate than the second-order accurate SA2 method. The SA3 method gives exact result for the constant strain rate problem.

To verify the observations let us first analyze a case where the solution approaches the steady-state solution $\sigma^* = (E_0 - E_\infty)\lambda\dot{\varepsilon}_0$. When the strain increment is constant, the recursive relation (22) yields a geometric series and therefore the numerical solution can be expressed in a closed form. When time tends to infinity, i.e. $n \to \infty$, the solution is given by

$$\begin{aligned}\sigma^* &= (E_0 - E_\infty)\lambda\dot{\varepsilon}_0 \cdot \frac{\Delta t}{\lambda}\frac{\psi_1(\Delta t/\lambda)}{1-\psi_0(\Delta t/\lambda)} \\ &\equiv (E_0 - E_\infty)\lambda\dot{\varepsilon}_0 \cdot f(\Delta t/\lambda). \end{aligned} \tag{56}$$

The RK methods produce a correct limit value irrespective of the size of the time step. For the SA1 and SA2 methods $f(\Delta t/\lambda)$ decreases rapidly as $\Delta t/\lambda$ increases. In the stability limit of the forward Euler method we find that $f(2) \approx 0.31$ for the SA1 method and $f(2) \approx 0.85$ for the SA2 method.

In the transient phase we may expect the SA methods to perform reasonably well. This is illustrated in Fig. 5 where the relative errors after the first time step are shown. For small time steps the SA2 method is the most accurate. However, even the backward Euler method is more accurate than the SA2 method when the time step is large enough. For large time steps the best choice is the Lobatto IIIC method.

Finally, we point out that we may expect the integrators to perform similarly also in a constant stress rate case since in that case, too, the strain rate tends to a constant value after a transient phase.

4.4 Creep

In the case of creep, the exact amplification factor is $\exp(-\eta\Delta t/\lambda)$. The local error is given by

$$\begin{aligned}\sigma^*(t_{n+1}) - \sigma^*_{n+1} &= e^{-\eta\Delta t/\lambda}\sigma^*(t_n) - \sigma^*_{n+1} \\ &= e^{-\eta\Delta t/\lambda}\sigma^*(t_n) - \psi_0(\Delta t/\lambda)\sigma^*(t_n) \\ &\quad -\psi_1(\Delta t/\lambda)(E_0 - E_\infty)\Delta\varepsilon \\ &= e^{-\eta\Delta t/\lambda}\sigma^*(t_n) \\ &\quad -\Big(\psi_0(\Delta t/\lambda) + \psi_1(\Delta t/\lambda) \\ &\quad \times (1 - 1/\eta)(e^{-\eta\Delta t/\lambda} - 1)\Big)\sigma^*(t_n) \\ &\equiv (A_{\text{exact}} - A_{\text{num}})\sigma^*(t_n), \end{aligned} \tag{57}$$

where A_{num} can be viewed as the "local" amplification factor.

In the limit $\Delta t/\lambda \to \infty$ all of the methods are accurate except the trapezoidal method. However, the amplification factors behave rather differently as $\Delta t/\lambda$ increases. When η is small, the amplification factors of the SA1 and SA2 methods approach the limit value rapidly, whereas for the backward Euler, Lobatto IIIC and SA3 methods, a slower but smoother behavior is observed, see Fig. 6. From Fig. 6 it can also be seen that the trapezoidal method performs considerably well even for large $\Delta t/\lambda$. Clearly, for stress-based experiments, the retardation time $\tau = \lambda/\eta > \lambda$, which is a time constant of the creep compliance, characterizes the stiffness of the problem. Consequently, the stability of the integrator of the viscoelastic model should be tested for a relaxation type problem rather than for a creep type problem.

For a nearly elastic material, the SA methods perform considerably better than the RK methods. This is shown in Fig. 7.

5 Multiaxial material model

5.1 Material model

We consider an isotropic constitutive model where the total stress $\boldsymbol{\sigma} = [\sigma_{11}\ \sigma_{22}\ \sigma_{33}\ \sigma_{12}\ \sigma_{13}\ \sigma_{23}]^{\mathrm{T}}$ and strain $\boldsymbol{\varepsilon} = [\varepsilon_{11}\ \varepsilon_{22}\ \varepsilon_{33}\ \varepsilon_{12}\ \varepsilon_{13}\ \varepsilon_{23}]^{\mathrm{T}}$ are decomposed into deviatoric and volumetric parts

$$\boldsymbol{\sigma}(t) = \boldsymbol{s}(t) + \mathbf{m}p(t), \tag{58}$$

$$\boldsymbol{\varepsilon}(t) = \boldsymbol{e}(t) + \frac{1}{3}\mathbf{m}\phi(t), \quad \mathbf{m} = [1\ 1\ 1\ 0\ 0\ 0]^{\mathrm{T}}, \tag{59}$$

where $\boldsymbol{s}$ is the deviatoric stress, $p = \frac{1}{3}\mathbf{m}^{\mathrm{T}}\boldsymbol{\sigma}$ is the mean stress, $\boldsymbol{e}$ is the deviatoric strain and $\phi = \mathbf{m}^{\mathrm{T}}\boldsymbol{\varepsilon}$ is the volume change. The deviatoric stress is given by

$$\boldsymbol{s}(t) = 2\int_0^t G(t-\tau)\dot{\boldsymbol{e}}(\tau)d\tau, \tag{60}$$

where $G(t)$ is the shear modulus and the mean stress is given by

$$p(t) = \int_0^t K(t-\tau)\dot{\phi}(\tau)d\tau, \tag{61}$$

where $K(t)$ is the bulk modulus. We assume that the bulk and shear moduli are given by

$$\begin{aligned} K(t) &= K_\infty + (K_0 - K_\infty)e^{-t/\lambda_K}, \\ G(t) &= G_\infty + (G_0 - G_\infty)e^{-t/\lambda_G}. \end{aligned} \tag{62}$$

Corresponding compliances for bulk and shear are

$$\begin{aligned} B(t) &= B_0 + (B_\infty - B_0)(1 - e^{-t/\tau_B}), \\ J(t) &= J_0 + (J_\infty - J_0)(1 - e^{-t/\tau_J}), \end{aligned} \tag{63}$$

where

$$B_0 = \frac{1}{K_0}, \qquad B_\infty = \frac{1}{K_\infty}, \qquad \tau_B = \lambda_K\frac{K_0}{K_\infty}, \tag{64}$$

$$J_0 = \frac{1}{G_0}, \qquad J_\infty = \frac{1}{G_\infty}, \qquad \tau_J = \lambda_G\frac{G_0}{G_\infty}. \tag{65}$$

5.2 Stress integration procedure

The numerical solution for stress is given by

$$\begin{aligned}\boldsymbol{\sigma}_{n+1} &= \boldsymbol{s}_{n+1} + \mathbf{m}p_{n+1} \\ &= 2G_\infty \boldsymbol{e}(t_{n+1}) + \boldsymbol{s}^*_{n+1} + K_\infty \mathbf{m}\phi(t_{n+1}) + \mathbf{m}p^*_{n+1},\end{aligned} \tag{66}$$

in which

$$\begin{aligned}\boldsymbol{s}^*_{n+1} &= \psi_0(\Delta t/\lambda_G)\boldsymbol{s}^*_n + 2\psi_1(\Delta t/\lambda_G)(G_0 - G_\infty)\Delta \boldsymbol{e}, \\ p^*_{n+1} &= \psi_0(\Delta t/\lambda_K)p^*_n + \psi_1(\Delta t/\lambda_K)(K_0 - K_\infty)\Delta\phi,\end{aligned} \tag{67}$$

where the functions $\psi_0(z)$ and $\psi_1(z)$ for the SA and RK methods are given in Table 1.

The consistent tangent operator, which will be needed in the forthcoming analysis and which is also very important when solving nonlinear finite element (FE) equations, is given by

$$\begin{aligned}\mathbf{C}_{\mathrm{T}} = \frac{\partial \boldsymbol{\sigma}_{n+1}}{\partial \boldsymbol{\varepsilon}(t_{n+1})} &= 2\Big[G_\infty + \psi_1(\Delta t/\lambda_G)(G_0 - G_\infty)\Big]\left[\mathbf{I} - \frac{1}{3}\mathbf{m}\mathbf{m}^{\mathrm{T}}\right] \\ &\quad + \Big[K_\infty + \psi_1(\Delta t/\lambda_K)(K_0 - K_\infty)\Big]\mathbf{m}\mathbf{m}^{\mathrm{T}}.\end{aligned} \tag{68}$$

where $\mathbf{I}$ is the identity matrix. To get a rough idea of the relative difference of the various tangent moduli we compare the volumetric part of the moduli. The volumetric part can be given in form

$$\Big[1 + \psi_1(\Delta t/\lambda_K)(1/\eta_K - 1)\Big]\mathbf{C}^*, \tag{69}$$

where $\eta_K = K_\infty/K_0 \in (0,1)$ is a dimensionless parameter and $\mathbf{C}^* = K_\infty \mathbf{m}\mathbf{m}^{\mathrm{T}}$ is a common factor. The relative difference can be now computed as a function of η_K and $\Delta t/\lambda_K$. The exact tangent operator is problem-dependent. Thus, the SA3 method, which is perhaps the most commonly used method in practical applications (Abaqus, 2004; Taylor, 2008) and is very accurate according to the local error analysis, was chosen as the reference method. The relative difference is shown in Fig. 8 using the value $\eta_K = 0.1$ for the dimensionless parameter. It is seen that for small time steps the SA2 method is closest to the SA3 method. For the backward Euler and Lobatto IIIC methods the difference significantly decreases once the maximum difference is attained. Consequently, for large time steps the Lobatto IIIC method is closest to the SA3 method.

5.3 Uniaxial tension

We consider a problem where the isotropic material is subjected to uniaxial stress $\sigma_{11}(t) = \dot{\sigma}_0 t$ where $\dot{\sigma}_0 = 0.5$ kPa. In this case we try to find the solution for the volume change and for the deviatoric strain components. The exact solutions for the volume change and for the deviatoric strain component in 1-direction are given by

$$\phi(t) = \frac{1}{3}(B * \dot{\sigma}_{11})(t), \quad e_{11}(t) = \frac{1}{3}(J * \dot{\sigma}_{11})(t), \tag{70}$$

where $*$ is the convolution operator. The material parameters are given in Table 6.

The solution for the strain components is found by solving a residual equation

$$\boldsymbol{\sigma}(t_{n+1}) - \boldsymbol{\sigma}_{n+1}(\boldsymbol{\varepsilon}_{n+1}) = 0, \tag{71}$$

using the Newton-Raphson method

$$\boldsymbol{\varepsilon}_{n+1}^{k+1} = \boldsymbol{\varepsilon}_{n+1}^{k} + \mathbf{C}_{\mathrm{T}}^{-1}\left(\boldsymbol{\sigma}(t_{n+1}) - \boldsymbol{\sigma}_{n+1}(\boldsymbol{\varepsilon}_{n+1}^{k})\right). \tag{72}$$

where k is the iteration number, $\boldsymbol{\sigma}(t_{n+1})$ is the exact stress vector and $\boldsymbol{\sigma}_{n+1}$ is the computed stress vector. Since the residual equation is linear, the Newton-Raphson method converges in one iteration. Once convergence is achieved, the volume change and deviatoric strain components are computed and the internal stress variables are updated.

The relative error at time $t = 10$ s is shown as a function of the time step in Figs. 9 and 10. For the deviatoric part the problem is nonstiff and thus for the deviatoric strain component the first-order accurate SA1 and backward Euler methods produce largest errors. For the volume part the problem is stiffer, the time constants, λ_K and τ_B, are order of a second. Furthermore, at time $t = 10$ s the transient phase, due to the exponential function, has completely damped out. In this case the performance of the SA1 and SA2 methods decreases. Even for a time step of size 0.1 s the backward Euler is more accurate than the SA2 method. This is consistent with the observation made in Section 4.3. Further, we see that for the trapezoidal method the error drastically increases as the time step is increased from 1 s to 10 s. The Lobatto IIIC and SA3 methods behave similarly in both cases, the only difference is that the relative error is slightly higher for the Lobatto IIIC method.

5.4 FEM-example: beam with a tip load

A beam with a tip load $F(t) = F_0 H(t)$ is analyzed, see Fig. 11. This problem has been previously considered in References Poon and Ahmad (1998); Zocher and Groves (1997). The length L of the beam is 20 m and the beam has a rectangular cross-section of size 1 m $\times$ 1 m. The solution for the tip displacement, according to Euler-Bernoulli beam theory, is given by

$$w(t) = \frac{F_0 L^3}{27I}\Big[3J(t) + B(t)\Big], \tag{73}$$

where I is the area moment of inertia of the beam. The physical properties of the beam are given in Table 6.

The isotropic model was implemented in the commercial FE-code ABAQUS using the user subroutine UMAT. The step function $H(t)$ was modeled by a ramp history wherein the force was increased to a constant value in a single time increment of size 10^{-4} s. The size of the load F_0 was 1 N. A mesh consisting of $10 \times 10 \times 200$ elements was used in the analysis. The time step was fixed at 5 s.

The simulation results are shown in Fig. 12. The results are in accordance with the uniaxial creep case. Compared to the backward Euler, Lobatto IIIC and SA3 methods, the numerical solution of the SA1 and SA2 methods reaches the steady-state solution rapidly. Again, the trapezoidal method performs extremely well although the time step is relatively large compared to the relaxation times.

6 Concluding remarks

In this paper, the performance of various time integrators of the integral model of linear viscoelasticity was studied. Both analytical and numerical analyses were presented.

The main results can be summarized as follows:

- The difference between the SA3, L3C and Tr methods, and between the SA1 and bE methods is in the order of approximation of the exponential function.
- The bE and L3C methods are accurate for both a very small and a very large time step. For nonstiff problems, say $\Delta t/\lambda < 2$, the Tr method can be considered to be the best choice among the RK methods.
- According to the local error analysis, the accuracy of the RK methods depends strongly on whether the initial values are on the slow manifold or not.
- For stiff problems we may expect the SA3, L3C and bE methods to behave in a similar fashion. A similar conclusion can be drawn between the SA1 and SA2 methods.
- The SA3, L3C and bE methods seem to behave more smoothly than the SA1 and SA2 methods. This should be noted if a notable change is made in the size of the time step.
- The stability analysis should be performed for a relaxation type problem rather than for a creep type problem.
- As regards the asymptotically first-order accurate methods, the bE method is a better choice than the SA1 method.
- Considering the overall performance of the integrators, the SA3 method is a superior choice. However, the L3C method behaves very similarly to the SA3 method.

Finally, we would like to point out that the analysis was focused on the relaxation-based material model. That is, we assumed that the relaxation modulus is the known material function. For nonlinear models, such as Schapery's model, the creep-based material model is often used. The results derived herein cannot be directly extended to creep-based models.

Acknowledgements The authors wish to acknowledge the assistance of Matti Malinen from Kuava Ltd.

References

Abaqus: Abaqus/Standard, Theory Manual. Version 6.5. Hibbitt, Karlsson and Sorenson, Inc., Pawtucket (2004)

Argyris J., Doltsinis I.St., da Silva V.D.: Constitutive modelling and computation of non-linear viscoelastic solids. Part I: Rheological models and numerical integration techniques. Comput. Meth. Appl. Mech. Eng. 88, 135-163 (1991)

Beijer J.G.J., Spoormaker J.L.: Solution strategies for FEM analysis with nonlinear viscoelastic polymers. Comput. Struct. 80, 1213-1229 (2002)

Beylkin G., Keiser J., Vozovoi L.: A new class of time discretization schemes for the solution of nonlinear PDEs. J. Comput. Phys. 147, 362-387 (2002)

Boyd J.P.: Chebyshev and Fourier spectral methods. Dover, New York (2001).

Büttner J., Simeon B. Runge-Kutta methods in elastoplasticity. Appl. Numer. Math. 41, 443-458 (2002)

Cox S.M., Matthews P.C.: Exponential time differencing for stiff systems. J. Comput. Phys. 176, 430–455 (2002)

Czyz J.A., Szyszkowski W.: An efficient method for non-linear viscoelastic structural analysis. Comput. Struct. 37, 637-646 (1990)

Dooling, P.J, Buckley C.P., Hinduja S.: An intermediate model method for obtaining a discrete relaxation spectrum for creep data. Rheol. Acta 36, 472-482, (1997)

Feng, W.W.: A recurrence formula for viscoelastic constitutive equations. Int. J. Non-Linear Mech. 27, 675-678, (1992)

Goh S.M., Charalambides M.N., Williams J.G.: Determination of the constitutive constants of non-linear viscoelastic materials. Mech. Time-Depend. Mater. 8, 255-268 (2004)

Gramoll K.C., Dillard D.A., Brinson H.F.: A stable numerical solution method for in-plane loading of non-linear viscoelastic laminated orthotropic materials. Compos. Struct. 13, 251-274 (1989)

Hairer E., Wanner G.: Solving ordinary differential equations II, stiff and differential-algebraic problems. Springer, Berlin (1991)

Haj-Ali R.M., Muliana A.H.: Numerical finite element formulation of the Schapery non-linear viscoelastic material model. Int. J. Numer. Meth. Eng. 59, 25-45 (2004)

Henriksen M.: Nonlinear viscoelastic stress analysis - a finite element approach. Comput. Struct. 18, 133-139 (1984)

Herrman L.R., Peterson F.E.: A numerical procedure for viscoelastic stress analysis. In: Proceedings of the Seventh Meeting of ICRPG Mechanical Behavior Working Group, Orlando (1968)

Holzapfel G.A.: On large strain viscoelasticity: continuum formulation and finite element applications to elastomeric structures. Int. J. Numer. Meth. Eng. 39, 3903-3926 (1996)

Hsu S.Y., Jain S.K., Griffin O.H.: Verification of endochronic theory for nonproportional loading paths. J. Eng. Mech. 117, 110-131 (1991)

Kennedy T.C.: Nonlinear viscoelastic analysis of composite plates and shells. Compos. Struct. 41, 265-272 (1998)

Kirchner E., Kollmann F.G.: Application of modern time integrators to Hart's inelastic model. Int. J. Plast. 15, 647-666 (1999)

Kirchner E., Simeon B.: A higher-order time integration method for viscoplasticity. Comput. Meth. Appl. Mech. Eng. 175, 1-18 (1999)

Knauss W.G., Zhao J.: Improved relaxation time coverage in ramp-strain histories. Mech. Time-Depend. Mater. 11, 199-216 (2007)

Kouhia R., Marjamäki P., Kivilahti J.: On the implicit integration of rate-dependent inelastic constitutive models. Int. J. Numer. Meth. Eng. 62, 1832-1856 (2005)

Kværnø A.: Time integration methods for coupled equations. Department of Mathematical Sciences, Norwegian University of Science and Technology, Preprint Numerics No. 7 (2004)

Lai J., Bakker A.: 3-D schapery representation for non-linear viscoelasticity and finite element implementation. Comput. Mech. 18, 182-191 (1996)

Minchev B.V., Wright W.M.: A review of exponential integrators for first order semi-linear problems. Department of Mathematical Sciences, Norwegian University of Science and Technology, Preprint Numerics No. 2 (2005)

Oden J.T., Armstrong W.H.: Analysis of nonlinear, dynamic coupled thermoviscoelasticity problems by the finite element method. Comput. Struct. 1, 603-621 (1971)

Patlashenko I., Givoli D., Barbone P.: Time-stepping schemes for systems of Volterra integro-differential equations. Comput. Meth. Appl. Mech. Eng. 190, 5691-5718 (2001)

Poon H., Ahmad M.F.: A material point time integration procedure for anisotropic, thermo rheologically simple, viscoelastic solids. Comput. Mech. 21, 236-242 (1998)

Poon H., Ahmad M.F.: A finite element constitutive update scheme for anisotropic, viscoelastic solids exhibiting non-linearity of the schapery type. Int. J. Numer. Meth. Eng. 46, 2027-2041 (1999)

Rivkin L., Givoli D.: An efficient finite element scheme for viscoelasticity with moving boundaries. Comput. Mech. 24, 503-512 (2000)

Schapery R.A.: On the characterization of nonlinear viscoelastic materials. Polymer. Eng. Sci. 9, 295-310 (1969)

Schapery R.A.: Nonlinear viscoelastic and viscoplastic constitutive equations based on thermodynamics. Mech. Time-Depend. Mater. 1, 209-240 (1997)

Schreyer H.L., Kulak R.F., Kramer J.M.: Accurate numerical solutions for elastic-plastic models. J. Pres. Vessel Tech. 101, 226-234 (1979)

Simo J.C., Kennedy J.G., Govindjee S.: Non-smooth multisurface plasticity and viscoplasticity. Loading/unloading conditions and numerical algorithms. Int. J. Numer. Meth. Eng. 26, 2161-2185 (1988)

Simo J.C., Hughes T.J.R.: Computational inelasticity. Springer, New York (1998)

Sorvari J., Malinen M.: On the direct estimation of creep and relaxation functions. Mech. Time-Depend. Mater. 11, 143-157 (2007)

Taylor R.L., Pister K.S., Goudreau G.L.: Thermomechanical analysis of viscoelastic solids. Int. J. Numer. Meth. Eng. 2, 45-59 (1970)

Taylor R.L.: FEAP - a finite element analysis program, version 8.2, theory manual. Department of Civil and Environmental Engineering, University of California at Berkeley (2008).

Touati D., Cederbaum G.: Stress relaxation of nonlinear thermoviscoelastic materials predicted from known creep. Mech. Time-Depend. Mater. 1, 321-330 (1998)

Zienkiewicz O.C., Watson M., King I.P.: A numerical method of visco-elastic stress analysis. Int. J. Mech. Sci. 10, 807-827 (1968)

Zienkiewicz O.C., Taylor R.L.: The finite element method. Butterworth-Heinemann, Oxford (2000)

Zocher M.A., Groves S.E.: A three-dimensional finite element formulation for thermo-viscoelastic orthotropic media. Int. J. Numer. Meth. Eng. 40, 2267-2288 (1997)

Østerby O.: Five ways of reducing the Crank-Nicolson oscillations. BIT Numer. Math. 43, 811-822 (2003)

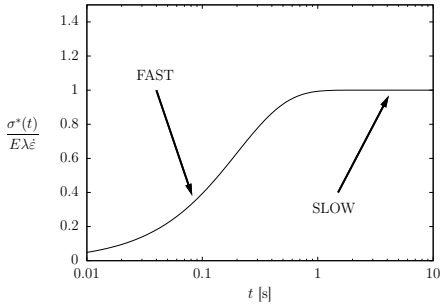

Fig. 1 Fast and slow manifolds in a case of constant strain-rate loading, i.e. $\dot{\varepsilon}$ = constant, $\lambda = 0.2$.

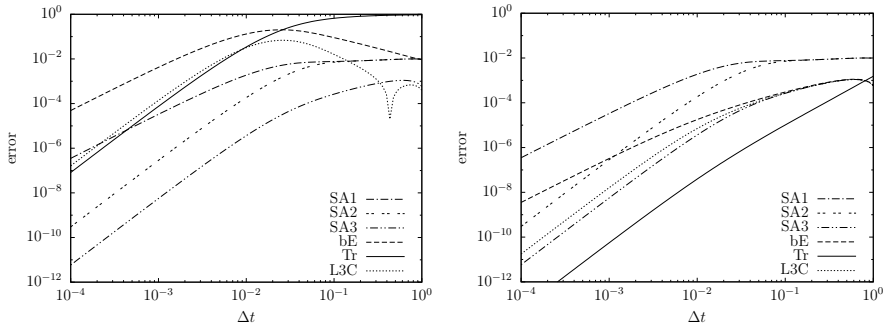

Fig. 2 The absolute value of the error for the internal stress after one time step ($\lambda = 10^{-2}$). (a) the initial value is off the slow manifold, (b) the initial value is on the slow manifold.

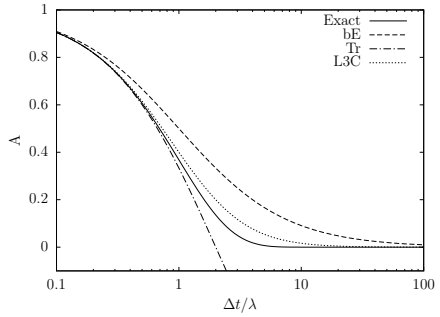

Fig. 3 Amplification factors in the relaxation problem.

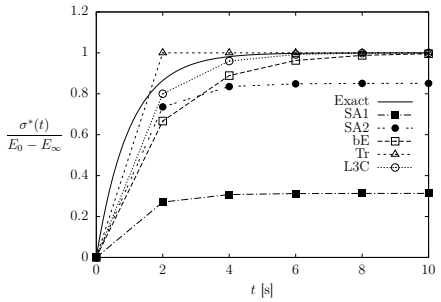

Fig. 4 Constant strain-rate loading ($\dot{\varepsilon}_0 = 1\ \mathrm{s}^{-1}$, $\lambda = 1$ s).

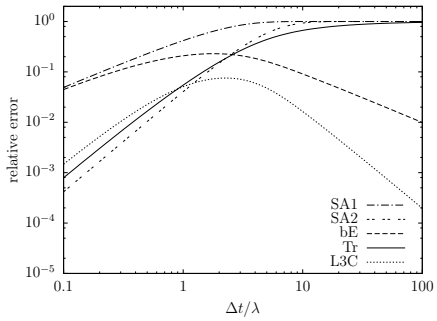

Fig. 5 Relative error after first time step in the constant strain rate loading case.

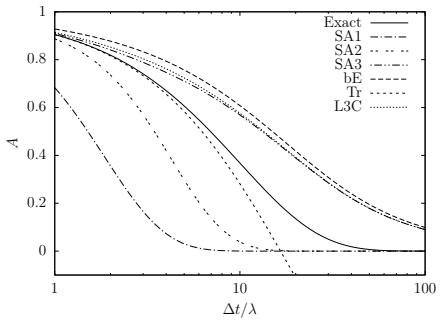

Fig. 6 Amplification factors in the creep problem, $\eta = 0.1$.

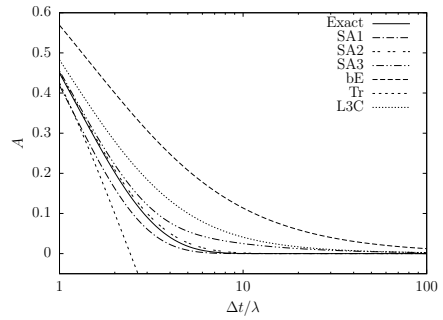

Fig. 7 Amplification factors in the creep problem, $\eta = 0.8$.

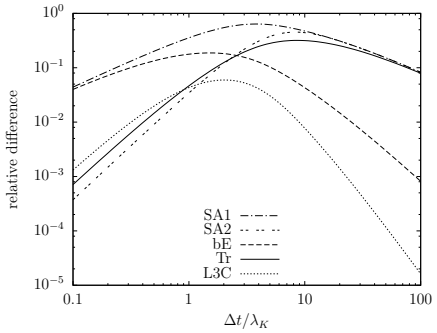

Fig. 8 Relative difference in tangent moduli, $\eta_K = 0.1$.

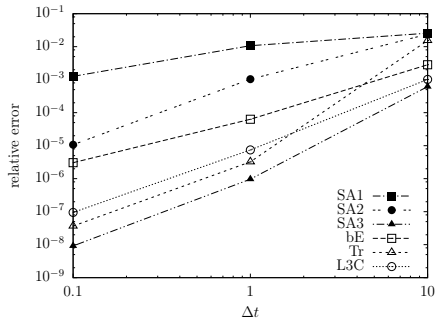

Fig. 9 Relative error in ϕ at time $t = 10$ s.

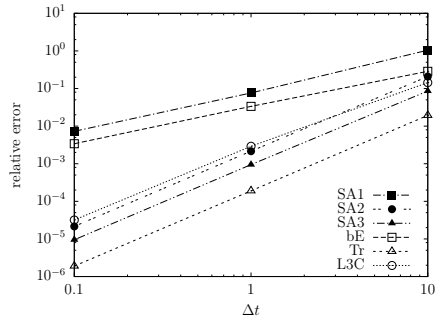

Fig. 10 Relative error in e_{11} at time $t = 10$ s.

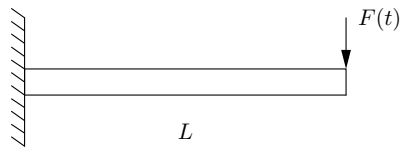

Fig. 11 Beam with a tip load.

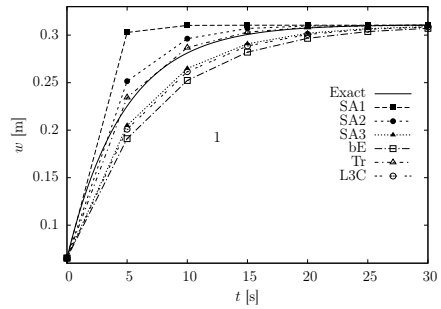

Fig. 12 Tip displacement.

Table 1 Functions $\psi_k(z)$ for the numerical methods.

	ψ_0	ψ_1
SA1	e^{-z}	e^{-z}
SA2	e^{-z}	$e^{-z/2}$
SA3	e^{-z}	$\frac{1-e^{-z}}{z}$
bE	$\frac{1}{1+z}$	$\frac{1}{1+z}$
Tr	$\frac{1-z/2}{1+z/2}$	$\frac{1}{1+z/2}$
L3C	$\frac{1}{1+z+z^2/2}$	$\frac{1}{1}\frac{1+z/2}{1+z+z^2/2}$

Table 2 Error functions $\mathcal{E}_k(z)$ for the methods when $z << 1$.

	$\mathcal{E}_0$	$\mathcal{E}_1$	$\mathcal{E}_2$
SA1	0	$\frac{1}{2}z + \mathcal{O}(z^2)$	$\frac{1}{3}z + \mathcal{O}(z^2)$
SA2	0	$\frac{1}{24}z^2 + \mathcal{O}(z^3)$	$\frac{1}{12}z + \mathcal{O}(z^2)$
SA3	0	0	$\frac{1}{12}z + \mathcal{O}(z^2)$
bE	$-\frac{1}{2}z^2 + \mathcal{O}(z^3)$	$\frac{1}{2}z + \mathcal{O}(z^2)$	$\frac{1}{3}z + \mathcal{O}(z^2)$
Tr	$\frac{1}{12}z^3 + \mathcal{O}(z^4)$	$-\frac{1}{12}z^2 + \mathcal{O}(z^3)$	$\frac{1}{12}z + \mathcal{O}(z^2)$
L3C	$-\frac{1}{6}z^3 + \mathcal{O}(z^4)$	$\frac{1}{6}z^2 + \mathcal{O}(z^3)$	$\frac{1}{12}z + \mathcal{O}(z^2)$

Table 3 Error functions $\widetilde{\mathcal{E}}_k(z)$ for the methods when $z << 1$.

	$\widetilde{\mathcal{E}}_1$	$\widetilde{\mathcal{E}}_2$	$\widetilde{\mathcal{E}}_3$
bE	0	$\frac{1}{2} + \mathcal{O}(z)$	$-\frac{1}{2z} + \mathcal{O}(1)$
Tr	0	0	$\frac{1}{12} + \mathcal{O}(z)$
L3C	0	$\frac{1}{4}z + \mathcal{O}(z^2)$	$-\frac{1}{6} + \mathcal{O}(z)$

Table 4 Error functions $\mathcal{E}_k(z)$ for the methods when $z >> 1$.

	$\mathcal{E}_0$	$\mathcal{E}_1$	$\mathcal{E}_2$
SA1	0	$\frac{1}{z} + \mathcal{O}(\frac{1}{z^2})$	$\frac{1}{z} + \mathcal{O}(\frac{1}{z^2})$
SA2	0	$\frac{1}{z} + \mathcal{O}(\frac{1}{z^2})$	$\frac{1}{z} + \mathcal{O}(\frac{1}{z^2})$
SA3	0	0	$\frac{1}{2z} + \mathcal{O}(\frac{1}{z^2})$
bE	$-\frac{1}{z} + \mathcal{O}(\frac{1}{z^2})$	$\frac{1}{z^2} + \mathcal{O}(\frac{1}{z^3})$	$\frac{1}{2z} + \mathcal{O}(\frac{1}{z^2})$
Tr	$1 + \mathcal{O}(\frac{1}{z})$	$-\frac{1}{z} + \mathcal{O}(\frac{1}{z^2})$	$\frac{1}{z^2} + \mathcal{O}(\frac{1}{z^3})$
L3C	$-\frac{2}{z^2} + \mathcal{O}(\frac{1}{z^3})$	$\frac{2}{z^3} + \mathcal{O}(\frac{1}{z^4})$	$\frac{1}{2z} + \mathcal{O}(\frac{1}{z^2})$

Table 5 Error functions $\widetilde{\mathcal{E}}_k(z)$ for the methods when $z >> 1$.

	$\widetilde{\mathcal{E}}_1$	$\widetilde{\mathcal{E}}_2$	$\widetilde{\mathcal{E}}_3$
bE	0	$\frac{1}{2z} + \mathcal{O}(\frac{1}{z^2})$	$\frac{1}{3z} + \mathcal{O}(\frac{1}{z^2})$
Tr	0	0	$\frac{1}{6z} + \mathcal{O}(\frac{1}{z^2})$
L3C	0	$\frac{1}{2z} + \mathcal{O}(\frac{1}{z^2})$	$\frac{1}{3z} + \mathcal{O}(\frac{1}{z^2})$

Table 6 Mechanical properties.

	Uniaxial tension	Beam with a tip load
K_0	10 MPa	0.38 MPa
K_∞	8 MPa	0.08 MPa
λ_K	1 s	1 s
G_0	6 MPa	0.19 MPa
G_∞	1 MPa	0.04 MPa
λ_G	5 s	1 s